Deformation potentials of the direct and indirect absorption edges of GaP

H. Mathieu, P. Merle, E. L. Ameziane, B. Archilla, and J. Camassel
Centre d'Etudes d'Electronique des Solides, Université des Sciences et Techniques du Languedoc, 34060-Montpellier-Cedex, France*

G. Poiblaud
La Radiotechnique Compelec, Route de La Delivrande, 14001-Caen-Cedex, France
(Received 17 March 1978)

We present uniaxial-stress experiments performed on the direct and indirect exciton spectrum of GaP. Two direct transitions (E_0 and $E_0+\Delta_0$) and three indirect phonon-assisted transitions (LA, TA, and TO phonon modes) have been investigated at 77 and 4.2°K, respectively. Very-high-stress conditions have been achieved in this work ($X = 19$ kbar) which correspond to an axial deformation $\delta l/l = 2\times10^{-2}$, reaching the elastic limit of the material. We have been able to determine all linear and nonlinear deformation potentials that describe the stress dependence of the topmost valence bands (Γ_7 and Γ_8) and of the lowest minima of the conduction band (Γ_6 and X_6). The stress splitting of the valence band is produced by (i) the orbital-strain interaction, which is described by two deformation potentials b_1 and d_1, and (ii) the stress-dependent spin-orbit interaction which is described by two extra parameters b_2 and d_2. We find $b = b_1+2\,b_2 = -(1.5\pm0.2)$ eV, $b_2 = +(0.2\pm0.2)$ eV, $d = d_1+2\,d_2 = -(4.6\pm0.2)$ eV, and $d_2 = +(0.3\pm0.2)$ eV. The effect of hydrostatic deformation is again interpreted in terms of two deformation potentials a_1 (orbital-strain interaction) and a_2 (strain-dependent spin-orbit interaction). They combine with two hydrostatic deformation potentials for the conduction band C_1 (at $k = 0$) and E_1 [at $k = (2\pi/a)$ (0,0,1)] to give the net pressure coefficients. We find $C_1+a_1+a_2 = -(9.9\pm0.3)$ eV, $E_1+a_1+a_2 = +(2.3\pm0.5)$ eV, and $a_2 = -(0.4\pm0.3)$ eV. The shear deformation potential E_2 of the indirect minimum of the conduction band has been obtained from the same series of measurements. We find $E_2 = +(6.3\pm0.9)$ eV. Lastly, the stress-induced coupling between the lowest minimum of the conduction band (X_6) and the next higher minimum (X_7) has been observed, and is described by a single deformation potential E_3. We find $|E_3| = 13\pm1.5$ eV.

I. INTRODUCTION

Under application of a uniaxial stress the cubic symmetry of standard semiconductors is reduced. This has long been recognized as a powerful tool to investigate the intrinsic properties of the unstressed crystals.[1] For example, uniaxial-stress experiments clearly demonstrate the ⟨111⟩ and ⟨100⟩ character of the lowest conduction-band minima in germanium and silicon, respectively. More recently, uniaxial-stress measurements performed on Ge and GaAs in the E_1, $E_1+\Delta_1$ interband absorption region[2] have provided the first conclusive evidence for the room-temperature existence of the Coulomb electron-hole interaction in this energy range. On the other hand, concerning impurity states, they have been used to investigate the nitrogen deep isoelectronic trap in GaP.[3-5] This level plays an important part in the luminescent properties of GaP and $GaAs_{1-x}P_x$ light-emitting diodes (LED). From the quenching of the deformation potentials associated with the luminescence line compared with those of the band edge, we would expect to get information concerning the admixture of Γ-X character in the impurity wave function and/or the coupling of the impurity with the host lattice. This is the so-called dynamic Jahn-Teller effect.[6] In order to get quantitative information, one needs accurate data concerning the deformation potentials associated with the band edges in undoped crystals. For GaP, there is only one result reported.[7] It deals with the shift of the indirect energy gap under [111] and [110] uniaxial compression, but no independent study of the direct E_0 and $E_0+\Delta_0$ transitions has been given. Moreover, these data extend only to 5 kbar and, in view of the low-stress value achieved in that work, Balslev was not able to account for the highly nonlinear stress-induced coupling between the topmost valence band (Γ_8 in Fig. 1) and the next spin-orbit split off band (Γ_7 in Fig. 1). Similarly, the stress-induced coupling between the two crystal-field-split X_6 and X_7 conduction-band extrema was ignored.

In this work, we report results obtained on a high-purity GaP crystal for stresses ranging up to 19 kbar. This corresponds to an axial component of the strain tensor $\delta l/l = 1.9\times10^{-2}$, reaching the elastic limit of the material. We present the first extensive investigation of the E_0, $E_0+\Delta_0$, and E_{ind} transitions under static uniaxial compressions directed along the [111], [001], and [110] crystallographic axes. To date, a similar set of data under very-high-stress conditions has only been reported for the indirect absorption edge of silicon, which is a prototype material.[8] For ger-

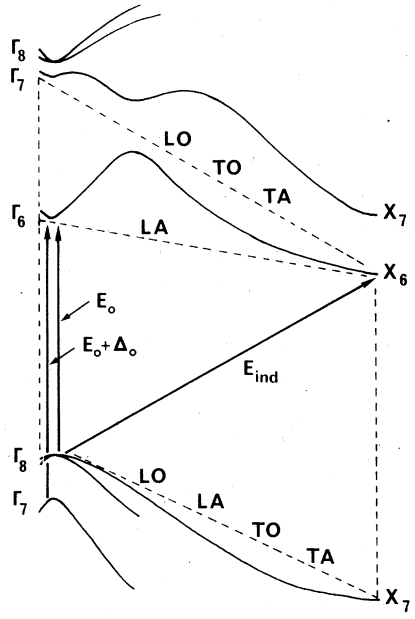

FIG. 1. Schematic band structure of GaP. At low temperature, the typical interband energies are: E_0 [P. J. Dean, G. Kaminsky, and R. B. Zetterstrom, J. Appl. Phys. 38, 3551 (1967)] = 2.87 eV (1.6 °K) and 2.86 eV (77 °K); E_{ind} (Ref. 12) = 2.346 eV (1.6 °K); Δ_0 (this work) = 90 meV; $\delta = X_7 - X_6$ (see Ref. 20) = 0.5 eV.

manium and most III-V compounds, including GaAs, all reported data have never exceeded 10 kbar.

In view of the large stress values achieved in this work, we have been able to determine accurately all deformation potentials of the direct and indirect gap of GaP. From the stress-induced displacements of the direct transitions E_0 and $E_0 + \Delta_0$, we get the orbital $(C_1 + a_1)$ and spin-dependent (a_2) hydrostatic deformation potentials of the lowest conduction band and topmost valence band at $k = 0$, together with the orbital (b_1, d_1) and spin-dependent (b_2, d_2) shear deformation potentials of the valence band. From the stress-induced splitting and the shift of the E_{ind} transitions, the hydrostatic deformation potential of the indirect gap $(E_1 + a_1 + a_2)$ and the shear deformation potential (E_2) of the lowest conduction-band minimum X_6 have been determined. We have also obtained the shear deformation potential (E_3) associated with the stress-induced coupling between the two X_6 and X_7 conduction bands. The orbital (b_1, d_1) and spin-dependent (b_2, d_2) shear deformation potentials of the topmost valence bands are independently obtained from the set of indirect transitions and compare well with the first $(E_0, E_0 + \Delta_0)$ determination.

This paper is organized as follows. In Sec. II we briefly discuss the experimental conditions. In Sec. III, we set the theoretical background and analyze the data. In Sec. IV, we discuss the experimental results.

II. EXPERIMENTAL

The single crystals used in this experiment were n-type nonintentionally doped GaP single crystals[9] grown by the liquid encapsulated Czochralski (LEC) method in a MSR 6 puller from Metals Research. Suitably pure starting GaP polycrystalline material was presynthesized by a gallium-solution growth process giving a residual doping concentration as low as 10^{15} cm^{-3}. Undoped LEC crystals pulled from this material had carrier concentrations in the range of 10^{15} cm^{-3} and mobilities higher than 150 cm^2 V^{-1} sec^{-1} at 300 °K. The central part of the ingots had a dislocation density of 10^4 cm^{-2}.

All samples were cut from a single ingot after x-ray orientation along the [111], [001], or [110] directions. This resulted in small parallelepiped samples of approximate dimensions $1 \times 1 \times 10$ mm^3. In order to ensure good stress homogeneity, the two narrow pressure faces were optically polished.

The indirect transitions (E_{ind}) were investigated at liquid-helium temperature by using wavelength-modulated transmission measurements.[7,8] The experimental resolution was kept around 2 meV. The direct transitions (E_0 and $E_0 + \Delta_0$) were recorded at 77 °K from a differential Schottky-barrier photovoltage method.[10] The Schottky barrier was realized by sputtering a semitransparent gold film on the sample surface. The photoresponse at a metal-semiconductor interface is known to depend mainly on the creation rate of free charge carriers in the semiconductor depletion layer. Provided this collection depth (W) is smaller than the absorption length (α^{-1}), the change in photovoltage directly reflects the change in absorption strength through the equation[10]

$$\Delta V = CW\Delta\alpha \ . \tag{1}$$

The advantages of the method are twofold: first, the sample itself acts as a good sensitivity photodetector; second, one can probe a much larger range of absorption strengths without changing the sample thickness. The absorption depth simply defines the active part. Comparing with E_{ind} measurements, where the full sample thickness is used ("volume" measurements), the E_0 and $E_0 + \Delta_0$ measurements appear like "surface" measurements—they provide a check on the stress homogeneity. Our stressing apparatus is a conventional one[11]: a lever arm lowers a stainless-steel rod which transmits the force to the sample cham-

ber. The samples are mounted between two optically flat pistons. A piezoelectric quartz transducer, positioned just below the sample, controls the strength.

By carefully optimizing the stressing surfaces, both on the samples and pistons, we have been able to reach a maximum value of 19 kbar in [111] direction, 14 kbar in [110] direction, and about 8 kbar in [001] direction. This corresponds to deformations along the stress direction of typically 1.9×10^{-2} for [111] stress and 0.8×10^{-2} for [001] stress. The trend in the maximum values that we report for GaP correlates surprisingly well with the one already reported for Silicon[8] (18, 14, and 10 kbar, respectively), and certainly corresponds with some elastic limit of these materials.

III. ANALYSIS OF DATA

The band structure of GaP has been well characterized, both from an experimental and a theoretical point of view (see Fig. 1). Neglecting the small linear-k terms, the maximum of the valence band occurs at $k=0$ and is characterized by a fourfold-degenerate Γ_8 multiplet (upper band) and a lower Γ_7 doublet, separated by the crystalline spin-orbit splitting Δ_0. The absolute minimum of the conduction band is characterized by three equivalent extrema X_6 at points $\vec{k}=(2\pi/a)\ (0,0,1)$. A direct miminum Γ_6, located at $k=0$, appears about 0.5 eV higher. The indirect absorption edge corresponds to phonon-assisted transitions from the valence-band maximum Γ_8 to the lowest conduction-band mimima X_6. These transitions are labeled TA, LA, and TO according to the branch of the phonons involved in the indirect processes.[12] The direct transitions $\Gamma_8\rightarrow\Gamma_6$ and $\Gamma_7\rightarrow\Gamma_6$ are labeled E_0 and $E_0+\Delta_0$, respectively.

Under uniaxial compression, the Γ_8 multiplet of the valence band splits and shifts, the Γ_7 doublet shifts, the Γ_6 minimum of the conduction band shifts, and the conduction-band valleys X_6 become nonequivalent (except for a [111] stress); they shift differently one from another (see Fig. 2). To first order in strain, these effects can be described by single deformation potentials. However, the splitting of the Γ_8 state is affected by both the orbital-strain interaction,[1] described by two independent deformation potentials (b_1 and d_1) and by the stress-dependent spin-orbit interaction,[13,14] which results in two additional independent deformation potentials (b_2 and d_2). The interband splitting of the conduction-band minima (X_6) is described by a shear deformation potential E_2. Finally, there is also a band shift due to the hydrostatic components. The hydrostatic shifts of the Γ_6 and X_6 conduction bands correspond, respectively, with the deformation potentials C_1 and E_1 and the hydrostatic shift of the Γ_8 and Γ_7 valence bands with the deformation potentials a_1+a_2 and a_1-2a_2, where a_1 is the hydrostatic orbital part and a_2 the hydrostatic stress-dependent spin-orbit interaction. In addition to the linear shifts and splitting of the X_6 conduction-band valleys, there exists a nonlinear contribution due to the stress-induced mixing between X_6 and X_7 (the next higher conduction-band minimum). This effect is small and can be described by an additional shear deformation potential E_3.

A. Direct transitions

If one neglects the stress-induced coupling between the Γ_6 conduction band and the Γ_8 ($M_j=\pm\frac{1}{2}$)

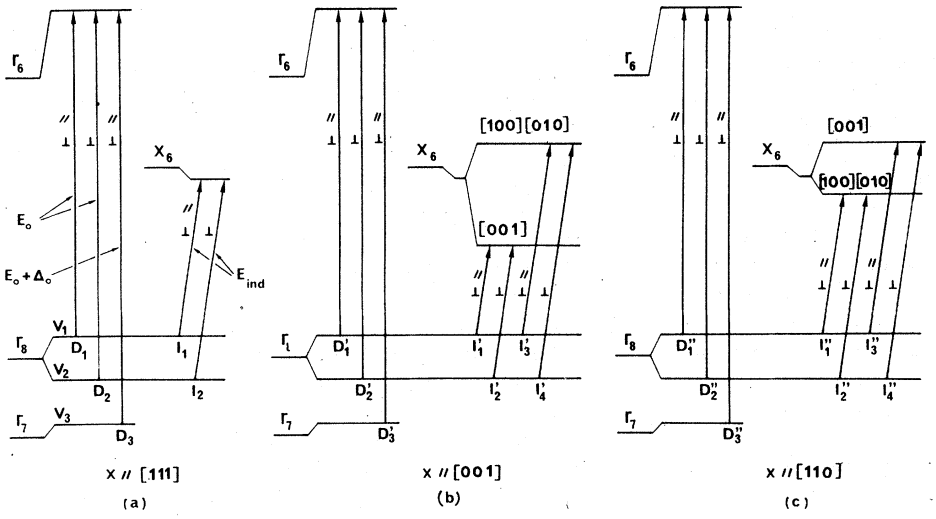

FIG. 2. Schematic illustrations of the strain effect on the band extrema for [111], [100] and [110] stresses. For $\vec{X}\parallel[111]$, we find indentical numbers of direct (D_1, D_2) and indirect (I_1, I_2) components. This is no longer true for [001] and [110] stress directions where the degeneracy of the three indirect conduction-band minima is lifted. This gives four possible transitions per phonon which we label I_1', I_2', I_3', and I_4' for $\vec{X}\parallel[001]$ and I_1'', I_2'', I_3'', and I_4'' for $\vec{X}\parallel[110]$.

valence band, the energy displacement of the Γ_6 minimum is linear in strain and may be written

$$\Delta C = C_1(e_{xx}+e_{yy}+e_{zz}), \tag{2}$$

where e_{ij} denotes the strain-tensor components.

For the total Γ_{15} valence band ($\Gamma_8+\Gamma_7$ in Fig. 2) the perturbation Hamiltonian is well known[1,8,13,15] and may be written

$$H = H_{SO} + H_1 + H_2, \tag{3}$$

where H_{SO} and H_2 are the stress-free and stress-dependent spin-orbit Hamiltonian, respectively, and H_1 is the orbital-strain Hamiltonian.

It is known[1,13] that H_1 and H_2 are given by

$$\begin{aligned} H_1 = &-a_1(e_{xx}+e_{yy}+e_{zz}) - 3b_1[(L_x^2 - \tfrac{1}{3}L^2)e_{xx} + \text{c.p.}] \\ &- \sqrt{3}\,d_1[(L_xL_y + L_yL_x)e_{xy} + \text{c.p.}] \end{aligned} \tag{4}$$

$$\begin{aligned} H_2 = &-a_2(e_{xx}+e_{yy}+e_{zz})(\vec{L}\cdot\vec{\sigma}) \\ &- 3b_2[(L_x\sigma_x - \tfrac{1}{3}\vec{L}\cdot\vec{\sigma})e_{xx} + \text{c.p.}] \\ &- \sqrt{3}\,d_2[(L_x\sigma_y + L_y\sigma_x)e_{xy} + \text{c.p.}], \end{aligned} \tag{5}$$

where $\vec{L}$ is the angular momentum operator, $\vec{\sigma}$ is the Pauli matrix, and c.p. denotes cyclic permutation with respect to the indices x, y, and z. The quantities a_1, b_1 and d_1 (a_2, b_2 and d_2), already defined, are orbital (spin-dependent) deformation potentials.

1. [111] stress

The strain-tensor components e_{ij} are

$$\begin{aligned} &e_{xx} = e_{yy} = e_{zz} = \tfrac{1}{3}(S_{11}+2S_{12})X, \\ &e_{xy} = e_{yz} = e_{zx} = \tfrac{1}{6}S_{44}X. \end{aligned} \tag{6}$$

S_{11}, S_{12}, and S_{44} are the elastic compliance coefficients. Their values for GaP are, in units of 10^{-6} bar^{-1} (Ref. 16),

$$S_{11} = 0.973, \quad S_{12} = -0.299, \quad S_{44} = 1.419.$$

Taking the valence-band wave functions in the $|J, M_J\rangle$ representation and the quantization axis along the stress direction,[8] the Hamiltonian matrix of Eqs. (4) and (5) becomes

$$\begin{array}{c} \left|\tfrac{3}{2},\tfrac{3}{2}\right\rangle_{111} \quad \left|\tfrac{3}{2},\tfrac{1}{2}\right\rangle_{111} \quad \left|\tfrac{1}{2},\tfrac{1}{2}\right\rangle_{111} \\ \left|\begin{array}{ccc} -\Delta V_H - D & 0 & 0 \\ 0 & -\Delta V_H + D & \sqrt{2}\,D' \\ 0 & \sqrt{2}\,D' & -\Delta_0 - \Delta V_H' \end{array}\right| \end{array}, \tag{7}$$

where

$$\begin{aligned} &\Delta V_H = (a_1+a_2)(S_{11}+2S_{12})X = a(S_{11}+2S_{12})X, \\ &\Delta V_H' = (a_1-2a_2)(S_{11}+2S_{12})X = a'(S_{11}+2S_{12})X, \\ &D = (1/2\sqrt{3})(d_1+2d_2)S_{44}X = (d/2\sqrt{3})S_{44}X, \\ &D' = (1/2\sqrt{3})(d_1-d_2)S_{44}X = (d'/2\sqrt{3})S_{44}X. \end{aligned}$$

Diagonalizing the above matrix, we get [with the usual approximation, $8D'^2 \ll (\Delta_0 - V_H + V_H' + D)^2$] the following expressions for the stress dependence of the lowest direct transitions:

$$\begin{aligned} &D_1 = A_0 - D - 2D'^2/(\Delta_0' + D), \\ &D_2 = A_0 + D, \\ &D_3 = A_0' + 2D'^2/(\Delta_0' + D), \end{aligned} \tag{8}$$

where

$$\begin{aligned} &A_0 = \Delta C + \Delta V_H = (C_1 + a_1 + a_2)(S_{11}+2S_{12})X, \\ &A_0' = \Delta C + \Delta V_H' = (C_1 + a_1 - 2a_2)(S_{11}+2S_{12})X, \\ &\Delta_0' = \Delta_0 - \Delta V_H + \Delta V_H' = \Delta_0 - 3a_2(S_{11}+2S_{12})X. \end{aligned}$$

A_0 is the hydrostatic pressure coefficient of the direct E_0 transition and A_0' is the pressure coefficient of the spin-orbit split-off transition $E_0+\Delta_0$. Their difference, $A_0 - A_0' = 3a_2(S_{11}+2S_{12})X$, gives the hydrostatic part of the strain-dependent spin-orbit interaction. All stress dependences are listed in Table I.

The three transitions D_1, D_2, and D_3 are schematically drawn in Fig. 2(a). Two of them, D_1 and D_3, correspond to both $\vec{E} \parallel \vec{X}$ and $\vec{E} \perp \vec{X}$ polarizations and should exhibit the quadratic behavior predicted by Eqs. (8). The third one, D_2, forbidden for $\vec{E} \parallel \vec{X}$ polarization, displaces linearly versus stress.

In Fig. 3(a), we show typical experimental spectra for $X=0$ and $X=19$ kbar. The experimental line shape at $X=0$ is characteristic of the first-order derivative of an E_0 direct excitonic transition. The spin-orbit split-off exciton is collision broadened and was not resolved. We estimate the spin-orbit splitting parameter Δ_0 to be 90 ± 5 meV. At $X=19$ kbar, all three transitions D_1, D_2, and D_3 are clearly resolved and well identified; D_2, which corresponds to a pure P_{xy} state, did not appear when the polarization was parallel to X. We note the spectral resolution in Fig. 3(a); the larger stress achieved in this work ($X=19$ kbar) corresponds to a strain component $e_{111} \simeq 2\times10^{-2}$ and reached the elasticity limit of the material. However, the spectral lines, even in these conditions, were not strain broadened. Obviously this is a very satisfactory check of the internal strain homogeneity.

Figure 4 shows the experimental stress dependences obtained in both polarizations. We find identical results by plotting independently either the positive or negative singularities that appear in Fig. 3(a). Accordingly, in Figs. 4–6 we plot only their relative changes. The full line shows the best fit obtained from Eqs. (8). The analysis

TABLE I. Stress dependences obtained for the direct (E_0, $E_0+\Delta_0$) and indirect transitions.

Transition	Stress direction	[111]	[001]	[110]
E_0		$D_1=A_0-D-2D'^2/(\Delta_0'+D)$	$D_1'=A_0-B-2B'^2/(\Delta_0'+B)$	$D_1''=A_0-F-2F'^2/(\Delta_0'+F)$
		$D_2=A_0+D$	$D_2'=A_0+B$	$D_2''=A_0+F$
$E_0+\Delta_0$		$D_3=A_0'+2D'^2/(\Delta_0'+D)$	$D_3'=A_0'+2B'^2/(\Delta_0'+B)$	$D_3''=A_0'+2F'^2/(\Delta_0'+F)$
E_{ind}		$I_1=A_x-D-2D'^2/(\Delta_0'+D)-\frac{1}{8}H^2/\delta$	$I_1'=A_x-B+\frac{2}{3}G-2B'^2/(\Delta_0'+B)$	$I_1''=A_x-F+\frac{1}{6}G-2F'^2/(\Delta_0'+F)-\frac{1}{4}H^2/\delta$
		$I_2=A_x+D-\frac{1}{8}H^2/\delta$	$I_2'=A_x+B+\frac{2}{3}G$	$I_2''=A_x+F+\frac{1}{6}G-\frac{1}{4}H^2/\delta$
			$I_3'=A_x-B-\frac{1}{3}G-2B'^2/(\Delta_0'+B)$	$I_3''=A_x-F-\frac{1}{3}G-2F'^2/(\Delta_0'+F)-\frac{1}{4}H^2/\delta$
			$I_4'=A_x+B-\frac{1}{3}G$	$I_4''=A_x+F-\frac{1}{3}G-\frac{1}{4}H^2/\delta$

$A_0=(C_1+a_1+a_2)(S_{11}+2S_{12})X$, $A_0'=(C_1+a_1-2a_2)(S_{11}+2S_{12})X$, $A_x=(E_1+a_1+a_2)(S_{11}+2S_{12})X$;

$D=[(d_1+2d_2)/2\sqrt{3}]S_{44}X$, $B=(b_1+2b_2)(S_{11}-S_{12})X$, $F=\frac{1}{4}(B+3D)$, $G=E_2(S_{11}-S_{12})X$;

$D'=[(d_1-d_2)/2\sqrt{3}]S_{44}X$, $B'=(b_1-b_2)(S_{11}-S_{12})X$, $F'=\frac{1}{4}(B'+3D')$, $H=\frac{1}{2}E_3S_{44}X$;

$\Delta_0'=\Delta_0-3a_2(S_{11}+2S_{12})X$.

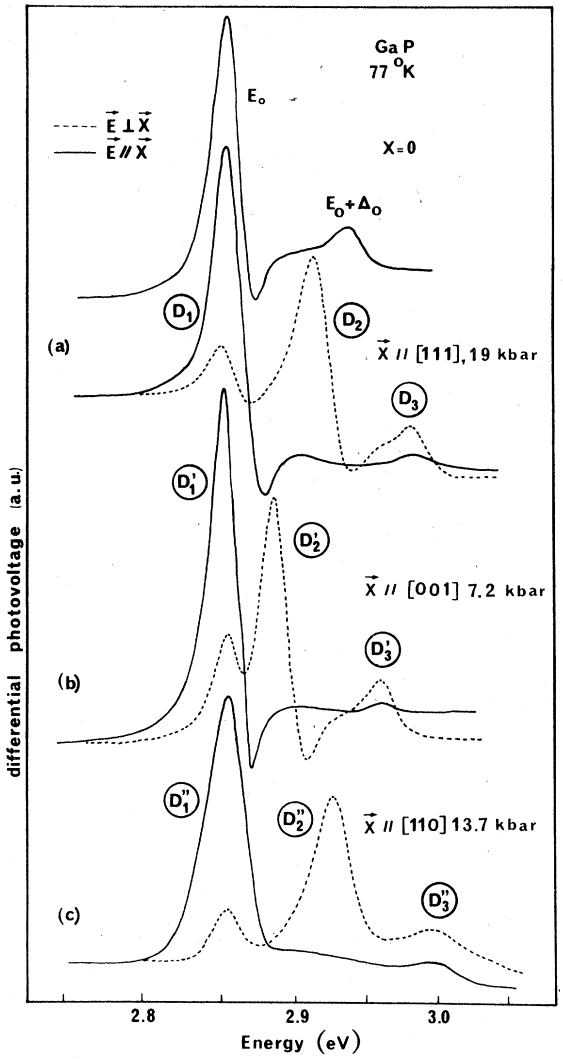

FIG. 3. Illustration of the stress-induced splitting of the direct E_0 and $E_0+\Delta_0$ transitions for both polarizations $\vec{E} \parallel \vec{X}$ and $\vec{E} \perp \vec{X}$. Note the appearance of the D_2 transition only for $\vec{E} \perp \vec{X}$ which identifies the V_2 band as the original level. Also note the very nice resolution for stresses as high as 19 kbar ([111] direction) or 14 kbar ([110] direction).

of data was conducted as follows. D_2 corresponds to the $J=\frac{3}{2}$, $M_j=\frac{3}{2}$ wave function (V_2 band in Fig. 2) and is linear through all the experimental range. On the other hand, for low-stress conditions we can neglect the quadratic terms in D_1 and D_3 which reduce to a linear dependence. This is shown as dashed lines in Fig. 4 and provides all inputs needed for a computer fit. The nonlinear dependence is then introduced and all parameters optimized until we get D_1 and D_3 in full agreement with experiment. We get in the [111] direction (in units of 10^{-6} eV bar^{-1})

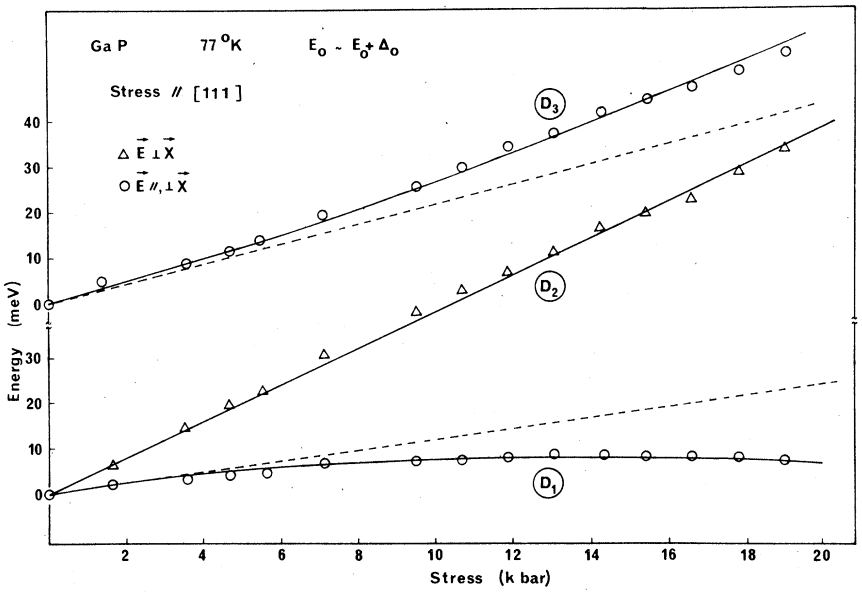

FIG. 4. Stress dependence of the three direct transitions originating from the Γ_{15} multiplet for $\vec{X} \parallel [111]$. Dashed line: linear component. Full line: best theoretical fit as discussed in the text.

$A_0 = 3.70$, $A_0' = 3.09$, $D = 2.00$, $D' = 2.21$.

All sets of experimental results are listed in Table II.

2. [001] stress

The strain-tensor components are

$$e_{xx} = e_{yy} = S_{12}X,$$
$$e_{zz} = S_{11}X, \tag{9}$$
$$e_{xy} = e_{yz} = e_{zx} = 0.$$

The hydrostatic parts (ΔV_c, ΔV_H, and $\Delta V_H'$) remain identical, but the shear terms D and D' change to[15]

$$B = (b_1 + 2b_2)(S_{11} - S_{12})X = b(S_{11} - S_{12})X,$$
$$B' = (b_1 - b_2)(S_{11} - S_{12})X = b'(S_{11} - S_{12})X. \tag{10}$$

The pressure dependence of the direct transitions is identical to Eqs. (8), but with B and B' replacing D and D', respectively:

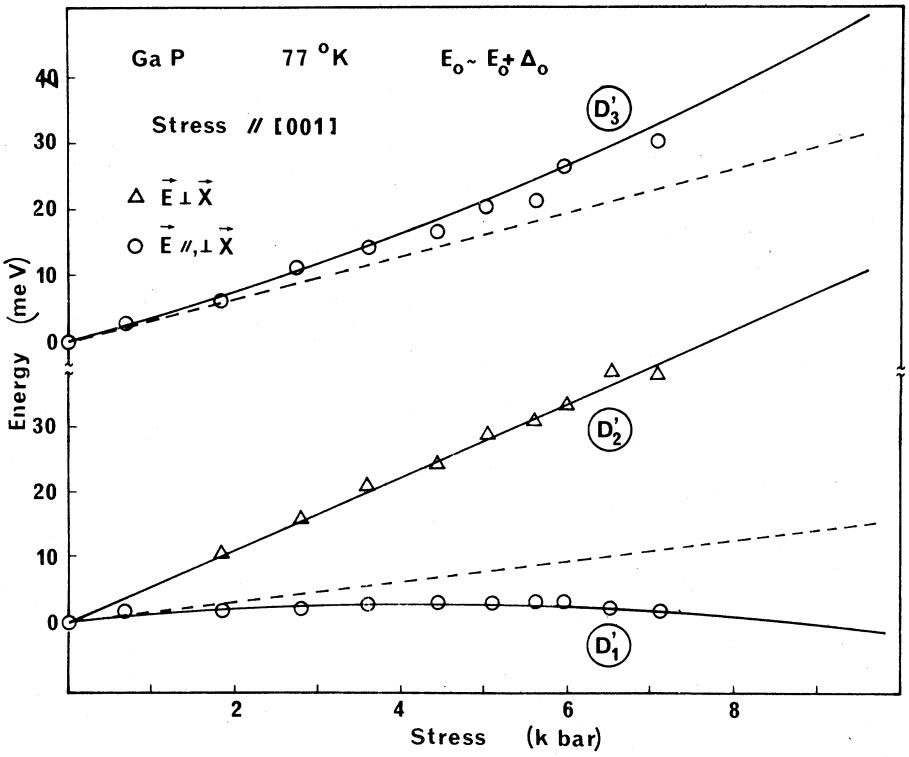

FIG. 5. Same as Fig. 4, but with $\vec{X} \parallel [001]$.

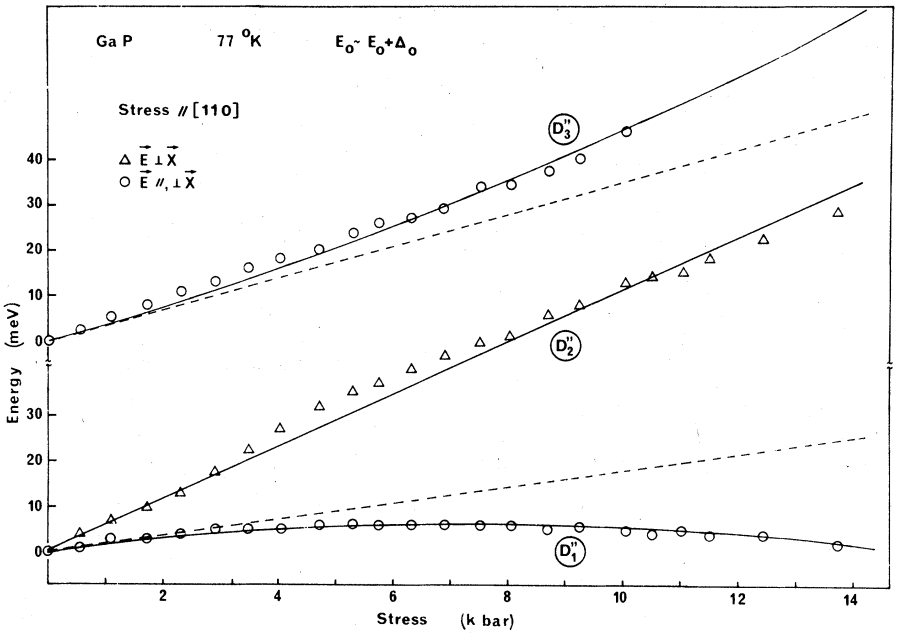

FIG. 6. Same as Fig. 4, but with $\vec{X} \parallel [110]$.

$$D_1' = A_0 - B - 2B'^2/(\Delta_0' + B),$$
$$D_2' = A_0 + B, \qquad (11)$$
$$D_3' = A_0' + 2B'^2/(\Delta_0' + B).$$

The three transitions, schematically drawn in Fig. 2(b), obey the same selection rules as they did in the [111] direction. This is illustrated on the experimental spectra of Fig. 3(b) for $\vec{E} \parallel \vec{X}$ and $\vec{E} \perp \vec{X}$. The corresponding stress dependence is displayed in Fig. 5. The dotted lines correspond again with the linear low-stress regime. The best theoretical fit, including the nonlinear quadratic shift, corresponds to (in units of 10^{-6} eV bar^{-1})

$$A_0 = 3.65, \quad A_0' = 3.30, \quad B = 2.05, \quad B' = 3.10.$$

Let us note the very close agreement obtained for the shear deformation of the valence band under [111] and [100] compressions. This isotropic splitting is further supported by our experimental results obtained in the [110] direction.

3. *[110] stress*

The strain-tensor components are

$$e_{xx} = e_{yy} = \tfrac{1}{2}(S_{11} + S_{12})X, \quad e_{zz} = S_{12}X,$$
$$e_{xy} = \tfrac{1}{4}S_{44}X, \quad e_{yz} = e_{zx} = 0.$$

TABLE II. Experimental values (units of 10^{-6} eV bar^{-1}) of the different parameters. The signs are given for a compression ($X < 0$). The nonlinear terms have been obtained with $\Delta_0 = 90$ meV and $\delta = 500$ meV.

Transition	Stress	A_0	A_0'	A_x	D	D'	B	B'	F	F'	G	H
	[111]	3.70	•••	•••	2.00	2.21	•••	•••	•••	•••	•••	•••
E_0	[001]	3.65	•••	•••	•••	•••	2.05	3.10	•••	•••	•••	•••
	[110]	3.81	•••	•••	•••	•••	•••	•••	1.95	2.60	•••	•••
	[111]	•••	3.10	•••	2.00 [a]	2.21 [a]	•••	•••	•••	•••	•••	•••
$E_0+\Delta_0$	[001]	•••	3.30	•••	•••	•••	2.05 [a]	3.10 [a]	•••	•••	•••	•••
	[110]	•••	3.50	•••	•••	•••	•••	•••	1.95 [a]	2.60 [a]	•••	•••
	[111]	•••	•••	−0.76	1.79	2.25	•••	•••	•••	•••	•••	9
E_{ind}	[001]	•••	•••	−1.03	•••	•••	1.80	2.35	•••	•••	−9.02	•••
	[110]	•••	•••	−0.75	•••	•••	•••	•••	1.98	2.40	−6.92	
average value		3.70 ±0.10	3.30 ±0.20	−0.85 ±0.20	1.90 ±0.10	2.25 0.10	1.95 ±0.20	2.70 ±0.40	1.96 ±0.20	2.50 ±0.30	−7.95 +1.1	9 ±1

[a] Value measured from the stress dependence of the E_0 structures.

When the stress was parallel to the [001] or [111] direction, the choice of the quantization axis along the stress direction led to a simple form for the matrix Hamiltonian. This is no longer the case when the stress is applied along a lower-symmetry axis such as the [110] axis. In this case, the matrix Hamiltonian is[8,15]

$$\begin{array}{c} \left|\tfrac{3}{2},\tfrac{3}{2}\right\rangle_{110} \quad \left|\tfrac{3}{2},\tfrac{1}{2}\right\rangle_{110} \quad \left|\tfrac{1}{2},\tfrac{1}{2}\right\rangle_{110} \\ \begin{vmatrix} -\Delta V_H - F & -\frac{1}{4}\sqrt{3}\,(B-D) & \frac{1}{4}\sqrt{6}\,(B'-D') \\ -\frac{1}{4}\sqrt{3}\,(B-D) & -\Delta V_H + F & \sqrt{2}F' \\ \frac{1}{4}\sqrt{6}\,(B'-D') & \sqrt{2}F' & -\Delta_0 - \Delta V_H' \end{vmatrix} , \end{array} \tag{12}$$

where $F=\frac{1}{4}(B+3D)$ and $F'=\frac{1}{4}(B'+3D')$.

In other words, the stress-induced mixing couples all V_1, V_2, and V_3 bands and should result in a nonlinear behavior for the three direct transitions. This is not the experimental situation for GaP (see Fig. 6). In this case, for nearly-stress-isotropic crystals $B=D$ and the matrix Hamiltonian of Eq. (12) reduces to a much simpler form. If we further neglect the spin-dependent mixing introduced by the matrix element $\frac{1}{4}\sqrt{6}\,(B'-D')$, the solutions are given by the set of Eqs. (8), replacing D and D' by F and F', respectively. They are listed in Table I, and we have worked under this assumption.

From our preceding results (see, for example, Table II), the approximation $B=D$ is well justified, but the neglect of the spin-dependent coupling term could appear arbitrary. This contribution should result in a nonlinear admixture of V_2 with V_3 and in a small quadratic shift of V_2. Neglecting all stress-induced admixtures between the unperturbed wave functions,[8] the magnitude of the quadratic component is $6(B'-D')^2/16\Delta_0$. With $B'=3\times10$ meV kbar^{-1}, $D'=2.21$ meV kbar^{-1}, and $\Delta_0=90$ meV, we compute a contribution: 4×10^{-3} meV kbar^{-2}. This is below our experimental range of accuracy, and completely justifies our approximation.

Figure 3(c) shows a typical experimental spectrum for $X\simeq14$ kbar with both polarizations, $\vec{E}\parallel\vec{X}$ and $\vec{E}\perp\vec{X}$. This permits identification of the transition D_2''. The stress dependences are displayed in Fig. 6 and, within experimental uncertainty, show the linear behavior expected for D_2''. This again supports the simplification of Eq. (12), and confirms the stress isotropic valence-band behavior already reported. The best fit is obtained with the following values of the parameters (in units of 10^{-6} eV bar^{-1}):

$$A_0=3.81,\quad A_0'=3.50,\quad F=1.95,\quad F'=2.60.$$

B. Indirect transitions

Under uniaxial [001] and [110] compressions, the degeneracy of the three equivalent X_6 minima is lifted. In the notation of Brooks,[17] the sum of hydrostatic (ΔX_H) shift and interband (ΔX_s) splitting is given by

$$\begin{aligned}\Delta X &= \Delta X_H + \Delta X_s \\ &= E_1(e_{xx}+e_{yy}+e_{zz}) \\ &\quad + E_2\hat{n}[\vec{e}-\tfrac{1}{3}(e_{xx}+e_{yy}+e_{zz})\vec{1}]\hat{n}\,,\end{aligned} \tag{13}$$

where $\hat{n}$ is a unit vector in the direction of the band extrema in k space, $\vec{1}$ is the unit diadic, and E_1 and E_2 are the hydrostatic and shear deformation potentials, respectively.

In addition to the linear effects, a nonlinear contribution exists due to the stress-induced coupling between the X_6 (X_1) and X_7 (X_3) conduction bands. The strain symmetry which can couple X_1 and X_3 is only X_3 and, owing to the irreducible representations of the strain components in the T_d symmetry group ($\Gamma_1+\Gamma_{12}+\Gamma_{15}$) and the compatibility relations between T_d and D_{2d}, we find that the only components of the strain tensor which have X_3 symmetry are the shear components e_{xy}, e_{yz}, and e_{zx}. Hence the nonlinear coupling between the conduction bands will be related only to [111] and [110] compressions. Introducing a shear deformation potential E_3, the 2×2 matrix Hamiltonian becomes simply[8-18]

$$\begin{array}{c} \left|X_6\right\rangle \quad \left|X_7\right\rangle \\ \begin{vmatrix} 0 & E_3 e_{xy} \\ E_3 e_{xy} & \delta \end{vmatrix} , \end{array} \tag{14}$$

where $\delta=X_7-X_6$ is the energy separation between the two crystal-field split minima. Diagonalizing this matrix and expanding to first order, we find for the nonlinear shift of the X_6 minimum

$$\Delta X' = -(E_3 e_{xy})^2/\delta\,. \tag{15}$$

1. [111] stress

This is the simplest situation. The degeneracy of the conduction band is not lifted, and, referring to the stress pattern for a direct transition, only the small quadratic term will modify the linear dependence expected for all transition originating from the $|\frac{3}{2},\frac{3}{2}\rangle$ valence band. From Eqs. (8)–(13) and (15), we obtain for the stress dependence of an indirect phonon-assisted transition (see Fig. 2)

$$\begin{aligned} I_1 &= A_X - D - 2D'^2/(\Delta_0'+D) - \tfrac{1}{9}H^2/\delta\,, \\ I_2 &= A_X + D - \tfrac{1}{9}H^2/\delta\,, \end{aligned} \tag{16}$$

where

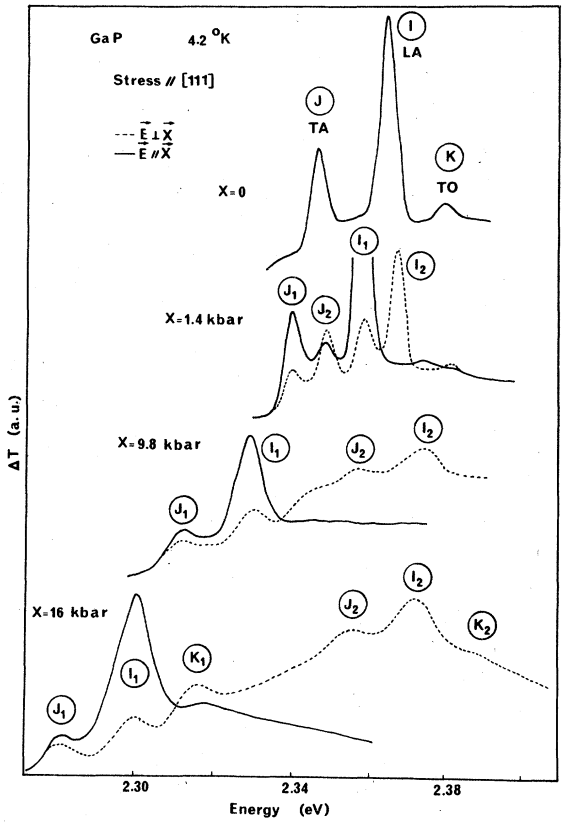

FIG. 7. Stress-induced splitting of the three indirect phonon-assisted transitions I, J, K at liquid-helium temperature for $\vec{E} \parallel \vec{X}$ and $\vec{E} \perp \vec{X}$. Note the identification of the I_2 transition (LA-phonon-assisted transition) which appears only when $\vec{E} \perp \vec{X}$ and follows exactly the selection rules observed for the direct transitions (Γ_6 intermediate state). The same is not true for the J_2 component (TA-phonon-assisted component) as shown at 1.4 kbar. This component, which involves both Γ_{15}^c and X_5^v intermediate states, appears in both polarizations $\vec{E} \perp \vec{X}$ and $\vec{E} \parallel \vec{X}$. At $X = 16$ kbar, the six lines appear well separated in two different series which originate for V_1 and V_2, respectively.

$$A_X = \Delta X_H + \Delta V_H = (E_1 + a_1 + a_2)(S_{11} + 2S_{12})X$$

and $H = \frac{1}{2}E_3 S_{44} X$. The complete stress pattern will be characterized by a number of lines which is twice the number of resolved phonons at $X = 0$.

In Fig. 7, we show an experimental wavelength-modulated transmission spectrum ($X = 0$) which displays three well-resolved phonon-assisted transitions (LA, TA, and TO). For clarity, we label I the LA-phonon-assisted transition, and use J for TA and K for TO. Under [111] compression the spectrum duplicates and becomes polarization dependent. At 16 kbar, two well-resolved sets of structures correspond with the splitting of the Γ_8 valence band. It is interesting to note that the transitions via the lowest direct conduction band (symmetry Γ_6) involve only phonons of symmetry X_1 (LA phonons). Thus the LA-phonon-assisted transition (i) will be strongest and (ii) will obey the same selection rules as does the E_0 transition. This is clearly seen on Fig. 7 for $X = 1.4$ kbar. The transition I_2, allowed for $\vec{E} \perp \vec{X}$, is totally forbidden for $\vec{E} \parallel \vec{X}$. The same is not true for J and K. Involving both $\Gamma_{7c} + \Gamma_{8c}$ and $X_{7v} + X_{6v}$ intermediate states, they obey different selection rules and are found in both polarizations. For convenience, we shall focus our investigation mainly on the strong LA structure whose identification is simpler.

In Fig. 8, we give the complete stress-dependence pattern of the three phonon-assisted transitions up to $X = 19$ kbar. The full lines show the best theoretical fit according to Eqs. (16), and the dotted lines illustrate the linear components. From the fit, we get (in units of 10^{-6} eV bar^{-1})

$$A_X = -0.76, \quad D = 1.79, \quad D' = 2.25, \quad H = 9 .$$

As expected from Eqs. (16), we find for this stress direction a small but definite nonlinear dependence of the transitions originating from the linear V_2 valence band. This is in sharp contrast with the result for the direct E_0 transitions, but would be hardly noticeable for compressions below 10 kbar.

2. *[001] stress*

This stress direction lifts the degeneracy of the three ⟨100⟩ ellipsoids in the conduction band and results in an intervalley splitting whose magnitude is obtained from Eq. (13):

$$\Delta X_s = G = E_2(S_{11} - S_{12})X . \tag{17}$$

Depending on signs, one ellipsoid ⟨001⟩ moves down by $\frac{2}{3}G$, while the other two ⟨100⟩ and ⟨010⟩ move up by $\frac{1}{3}G$. This situation is illustrated schematically in Fig. 2(b). For each phonon line, we get now four different branches (primed transitions) which correspond with two different valence bands and two different conduction bands. The corresponding stress dependences are obtained from Eqs. (8) and (17) and are listed in Table I. Two branches I_2' and I_4' originate from the $J = \frac{3}{2}$, $M_j = \frac{3}{2}$ valence band (V_2) and are strictly linear. The two other ones, I_1' and I_3', exhibit the nonlinear behavior characteristic of the $V_1 - V_3$ intervalence band mixing.

Typical experimental spectra are shown in Fig. 9. From the three phonon lines (I, J, K) resolved at $X = 0$, we expect 12 branches. Only eight have been resolved because of destructive interferences between the weak TA and TO phonon lines (J' and K') with the strong LA ones (I').

The complete stress-dependent pattern is shown in Fig. 10 for X up to about 8 kbar. Note the strong mixing of all experimental structures that appears at about $X = 2$ kbar. The polarization-

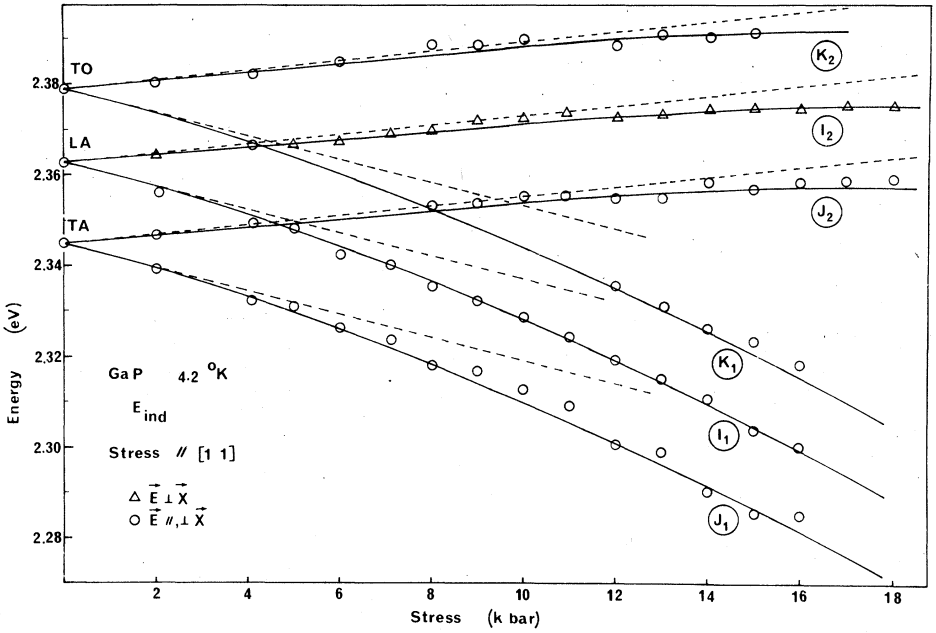

FIG. 8. Stress dependence of the six I_1-I_2, J_1-J_2, K_1-K_2 phonon-assisted transitions under uniaxial [111] compression. Because of the stress induced X_6-X_7 interconduction band mixing, all lines shift quadratically. The dashed lines correspond with the small stress linear regime and the full lines with the best theoretical fit as discussed in the text.

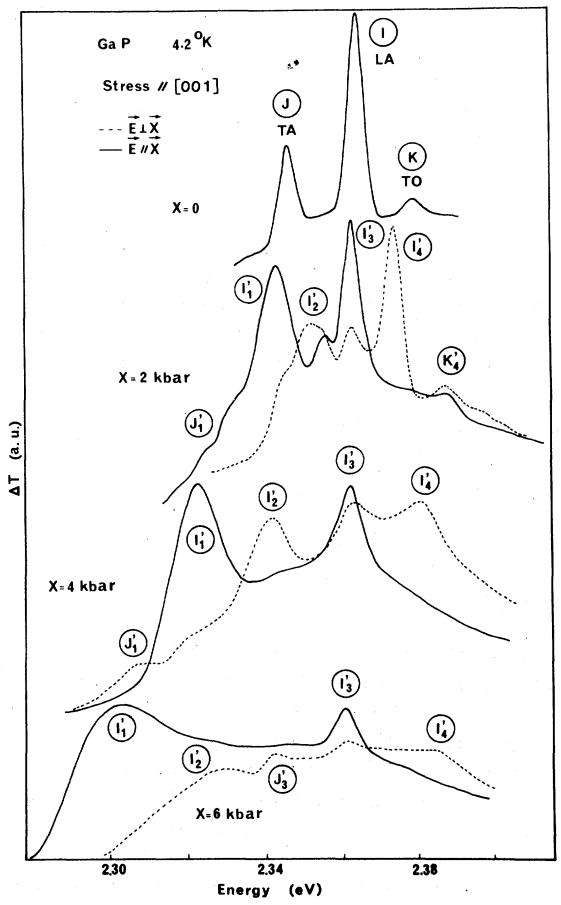

FIG. 9. Same as Fig. 7, but $\vec{X} \parallel [001]$. The maximum stress value reached in this crystallographic direction was about 8 kbar.

dependent spectra shown in Fig. 9 helped to clarify the data. The best theoretical fit is obtained with (in units of 10^{-6} eV bar^{-1})

$$A_X = -1.03, \quad B = 1.80, \quad B' = 2.35, \quad G = -9.02.$$

G has a negative sign which shows that under [001] compression for GaP, one ellipsoid moves down and two ellipsoids move up.

3. *[110] stress*

This is the most complex situation. For each phonon line (I, J, K) we find again four branches, but now, owing to the $X_6 - X_7$ stress-induced mixing, none of them is expected to shift linearly. The stress dependences expected from Eqs. (12), (13), and (14) are listed in Table I (double-primed transitions). Two of them (I_2'' and I_4'') originates from the V_2 valence band, and exhibit only the small conduction-band nonlinear mixing already introduced for $\vec{X} \parallel [111]$. This is hardly noticeable on experimental data below 12 kbar (see Fig. 8), and will be neglected in the analysis.

In Fig. 11 we give typical experimental data for $\vec{E} \parallel \vec{X}$ and $\vec{E} \perp \vec{X}$. Among the 12 components, only 9 have been resolved and analyzed with help of the polarization-dependent spectra.

Figure 12 shows the complete stress pattern obtained for this stress direction. Some components (K_4'', J_2'') are only poorly resolved. They disappear very rapidly or mix with the strong LA (I'') phonon branch. Some (K_2'', K_1'') were not found at low stress because of the complexity of the spectra and appear only above 6 kbar. The best

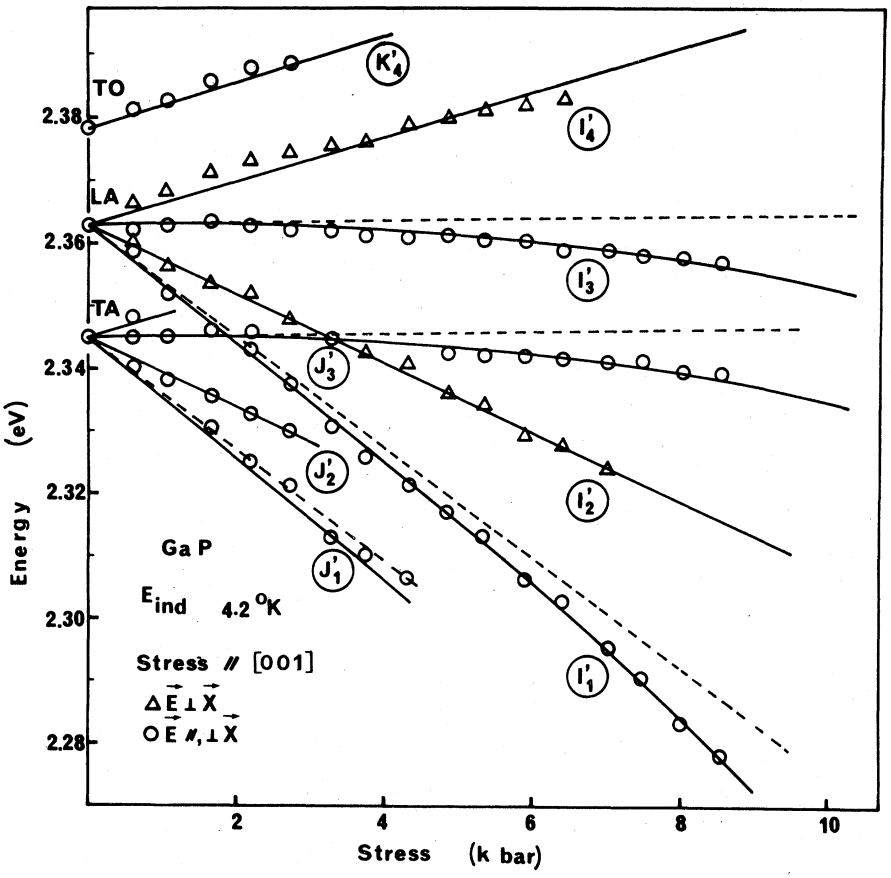

FIG. 10. Same as Fig. 8 but for $\vec{X} \parallel [001]$. In this stress direction there is no interconduction band mixing, and all levels which originate from V_2. (l'_2 and l'_4, for example) shift linearly vs X.

theoretical fit was obtained with (in units of 10^{-6} eV bar^{-1})

$$A_X = -0.75, \quad F = 1.98, \quad F' = 2.40, \quad G = -6.92.$$

IV. DISCUSSION

All parameters obtained from the fit of experimental data are listed in Table II and averaged to account for the experimental uncertainty. We have obtained three independent determinations of the hydrostatic-stress dependences A_0, A'_0, and A_x, and two independent determinations of the shear-stress dependence of the valence band B, D, B', and D' and of the lowest conduction band G. From expressions listed in Table I, together with the elastic compliance constant of Ref. 16, we obtain the deformation potentials listed in Table III.

We find for the hydrostatic deformation potential of the direct band gap at $k = 0$: $C_1 + a_1 + a_2 = -9.9 \pm 0.3$ eV, which corresponds to a pressure coefficient

$$\frac{dE_0}{dP} = -3(C_1 + a_1 + a_2)(S_{11} + 2S_{12})$$

of 11.1 ± 0.3 meV/kbar. Hydrostatic-pressure experiments[19] give 10.7 ± 1.1 meV/kbar, in excellent agreement with our experimental finding. In view of the strong similarities between all group IV and III-V compounds,[20] we can also compare with the stress dependence of the direct band edge in Ge and GaAs as obtained from recent uniaxial[2] and hydrostatic[21] measurements. For Ge and GaAs, Chandrasekhar and Pollak[2] report $C_1 + a_1 + a_2 = -10.6 \pm 0.8$ eV and -8.4 ± 0.8 eV, respectively. On the other hand, for GaAs Welber *et al.*[4] report $dE_0/dP = 12.6 \pm 0.1$ meV/kbar, which gives a deformation potential $C_1 + a_1 + a_2 = -9.8$ eV. All these values are in very good agreement with our experimental result for GaP.

The indirect band-gap hydrostatic deformation potential obtained is $E_1 + a_1 + a_2 = 2.3 \pm 0.5$ eV. The corresponding hydrostatic-pressure coefficient is $dE_{ind}/dP = -2.6 \pm 0.5$ meV/kbar. This value must be compared with (i) previous hydrostatic measurements which give[19-22] $dE_{ind}/dP = -1.1 \pm 0.1$ meV/kbar and (ii) uniaxial-stress measurements[7] which give -4.5 ± 1.5 meV/kbar. We have not been able to resolve the discrepancy between the different series of data, but we may compare it with recent hydrostatic stress measurements performed on the indirect band edge of silicon,[23] where the pressure coefficient was $dE_{ind}/dP = -1.41 \pm 0.06$

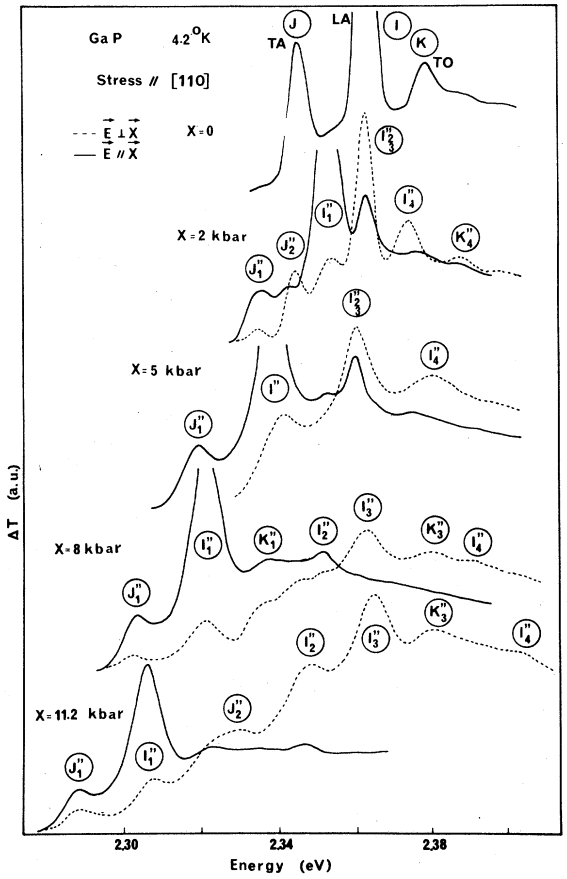

FIG. 11. Same as Fig. 7, but for $\vec{X} \parallel [110]$.

meV/kbar, which corresponds to $C_1 + a_1 + a_2 = 1.7$ eV. Within experimental uncertainty, this is in satisfactory agreement with our experimental finding.

The shear deformation potential of the conduction band $[k = (2\pi/a)(0, 0, 1)]$ is obtained from the average value $G = -(8 \pm 1)$ meV/kbar. We get $E_2 = 6.3 \pm 0.9$ eV in satisfactory agreement with the report $E_2 = 7 \pm 0.5$ given by Balslev.[7]

Owing to the high stresses reached in our experiment, we have been able to measure accurately the nonlinearities and then to determine independently the orbital (a_1, b_1, d_1) and spin-dependent (a_2, b_2, d_2) deformation potentials of the topmost valence bands, and to estimate the shear deformation potential E_3 associated with the stress-induced coupling between the two $X_6 - X_7$ conduction bands.

The values obtained for the valence-band deformation potentials $d = d_1 + 2d_2 = -4.6 \pm 0.2$ eV and $b = b_1 + 2b_2 = -1.5 \pm 0.2$ eV compare satisfactorily with (i) the deformation potential obtained in the linear approximation by Balslev, $d = -4.4 \pm 0.15$ eV and $b = -1.4 \pm 0.5$ eV, and (ii) most data previously reported for III-V compounds:

GaAs: $d = -4.55 \pm 0.25$ eV,

$b = -1.7 \pm 0.1$ eV (Ref. 2);

GaSb: $d = -4.2 \pm 0.2$ eV,

$b = -1.8 \pm 0.1$ eV (Ref. 24);

AlSb: $d = -4.3 \pm 0.4$ eV,

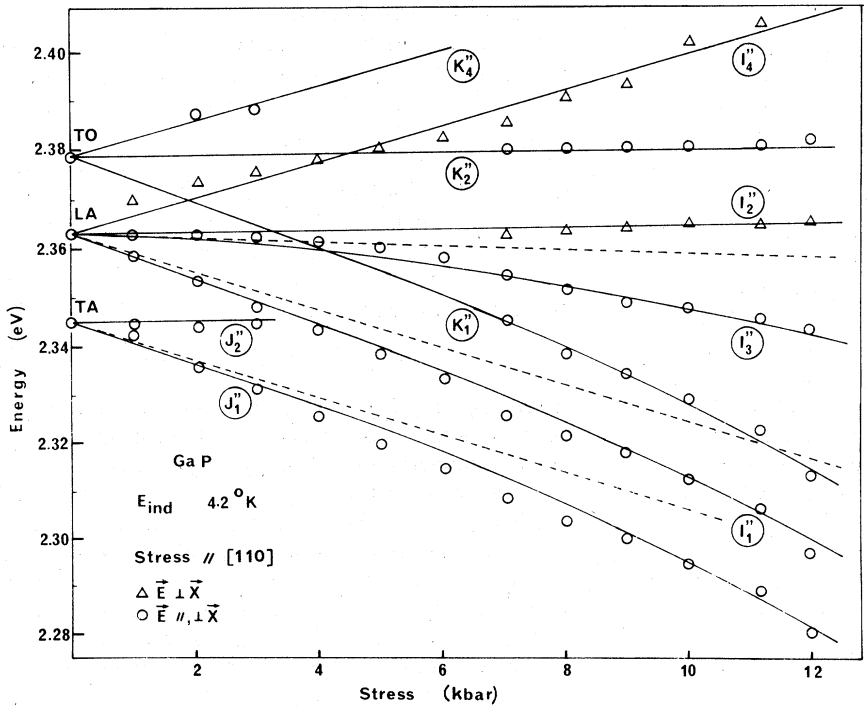

FIG. 12. Same as Fig. 8, but for $\vec{X} \parallel [110]$. The nonlinear X_6–X_7 interconduction band mixing is neglected in this stress direction.

TABLE III. Summary of the deformation potentials obtained for GaP and comparison with previous experimental results reported for GaP, Si, GaAs, and AlSb.

Transition	Deformation potentials (eV)	GaP This work	GaP Previous works	Si [c]	GaAs [d]	AlSb [e]
E_0	$c_1+a_1+a_2$	-9.9 ± 0.3	-9.5 ± 1.0 [a]		8.4 ± 0.8	-5.9 ± 1.2
$E_0+\Delta_0$	$c_1+a_1-2a_2$	-8.8 ± 0.6			8 ± 0.6	
	c_1+a_1	-9.5 ± 0.4				
	a_2	-0.4 ± 0.3		0		
E_{ind}	$E_1+a_1+a_2$	$+2.3\pm0.5$	$+1\pm0.1$ [a]	1.5 ± 0.3		2.2 ± 0.2
			$+3.7\pm0.6$ [b]			
	E_1+a_1	$+2.7\pm0.8$				
	$d=d_1+2d_2$	-4.6 ± 0.2	-4.4 ± 0.5 [b]	-4.85 ± 0.15	-4.55 ± 0.25	-4.3 ± 0.4
	$d'=d_1-d_2$	-5.5 ± 0.2			-5.5 ± 0.4	
E_0	d_1	-5.2 ± 0.2		4.9 ± 0.25	-5.2 ± 0.2	
	d_2	$+0.3\pm0.2$		-0.05 ± 0.25	$+0.35\pm0.15$	
and	$b=b_1+2b_2$	-1.5 ± 0.2	-1.4 ± 0.15 [b]	-2.1 ± 0.10	-1.7 ± 0.1	-1.35 ± 0.1
E_{ind}	$b'=b_1-b_2$	-2.1 ± 0.3			-2.6 ± 0.2	
	b_1	-1.9 ± 0.3		-1.95 ± 0.15	-2.35 ± 0.15	
	b_2	$+0.2\pm0.2$		-0.10 ± 0.15	$+0.3\pm0.1$	
E_{ind}	E_2	$+6.3\pm0.9$	$+7\pm0.5$	-8.6 ± 0.4		5.4 ± 0.3
	$\lvert E_3\rvert$	13 ± 1.5		$2(8\pm3)$		

[a] Reference 19.
[b] Reference 7.
[c] Reference 8.
[d] Reference 2.
[e] Reference 25.

$b=-1.35\pm0.1$ eV (Ref. 25).

The spin-dependent deformation potentials a_2, b_2, and d_2 have been obtained for the first time for GaP. We get $a_2=-0.4\pm0.3$ eV, $b_2=0.2\pm0.2$ eV, and $d_2=0.3\pm0.2$ eV. These results are in satisfactory agreement with the experimental values reported for germanium,[2] silicon,[8] and GaAs,[2] but all are an order of magnitude larger than the theoretical estimates.[13,14,26-29] From perturbation theory Hensel and Suzuki[13,14] show that different terms contribute to a_2, b_2, and d_2. They are (i) a "kinetic" term which derives simply from the scaling process in applying the Pikus-Bir transformation[1] to the coordinates, (ii) a term which depends on the change in crystal potential with strain, and (iii) negligible higher-order contributions. Within the deformable-ion approximation they estimate the kinetic contribution and obtain

$$a_2=-\tfrac{2}{9}\Delta_0 \quad \text{and} \quad b_2=d_2=\tfrac{1}{3}\Delta_0 .$$

With $\Delta_0=90$ meV, this gives for GaP the values

$$a_2=-0.020 \text{ eV} \quad \text{and} \quad b_2=d_2=0.030 \text{ eV},$$

which are about an order of magnitude lower than the experimental results.

We have attempted a rough estimate of the contribution which corresponds to the change in crystal potential neglected in the deformable-ion approximation. This term, which depends upon the strain-induced change of the crystal potential, can be readily estimated using the empirical tight-binding method.[30,31] The determination of the tight-binding parameters is relatively simple in cubic crystals,[31,32] and an explicit expression for the spin-orbit splitting Δ_0 at Γ has been derived[32]

$$\Delta_0=\tfrac{1}{2}(\Delta_a+\Delta_c)+\tfrac{1}{2}(\Delta_a-\Delta_c)(E_{p2}-E_{p1})/E_0' ,$$

where Δ_a, Δ_c, E_{p1}, and E_{p2} are the atomic spin-orbit values and p-state energies for the anion and cation, respectively. Taking[32] $\Delta_a=0.067$ eV, $\Delta_c=0.714$ eV, $E_{p1}=1.28$ eV, $E_{p2}=3.82$ eV, and $E_0'=5.20$ eV, one gets $\Delta_0=94$ meV, in excellent agreement with the experimental value $\Delta_0=90\pm5$ meV.

Let us assume that the contribution which dominates the change in Δ_0 comes only from a change in the coupling parameter V_{xx} which connects two p states originating from different atoms. A straightforward calculation gives

$$d(\Delta_0) = -\tfrac{1}{2}[(\Delta_a - \Delta_c)(E_{p2} - E_{p1})/E_0'^2]\, d(E_0') ,$$

where[32]

$$E_0' = (E_{p1} - E_{p2}\ \ \tfrac{1}{3}\Delta_a - \tfrac{1}{3}\Delta_c^2) + 4V_{xx}^2 .$$

The change in V_{xx} versus lattice parameter is obtained from the standard rule[33,34] $V_{xx} \sim d^{-2}$, which gives for a hydrostatic pressure $dV_x = -2V_{xx}\Delta d/d$, where d is the nearest-neighbor distance. The resulting contribution to a_2 is then

$$\Delta a_2 = 4(\Delta_a - \Delta_c)(E_{p2} - E_{p1})V_{xx}^2/9E_0'^3 ,$$

which gives $\Delta a_2 \sim 0.004$ eV. This contribution is again very small and cannot explain the discrepancy between the experimental results and the calculated values.

It is to note that the dependence of the spin-orbit Hamiltonian on uniaxial stress (described by the deformation potentials a_2, b_2, and d_2) where introduced by Hensel and Suzuki,[13,14] to explain the strain dependence of the hole effective masses in germanium. More recently, Aspnes and Cardona[35] indicate that the anomalous strain dependence of the cyclotron hole masses observed for Ge by Hensel and Suzuki are not due to a strain-dependent spin-orbit interaction, as suggested by these authors, but to orbital terms involving the higher conduction bands. Their calculations show that the splitting of the Γ_{15} valence band is not the only term that contributes significantly to the dependences of the valence-band masses on uniaxial stress. In fact, the stress dependence of these masses can be viewed as resulting largely from third-order perturbation terms involving the $\vec{k}\cdot\vec{p}$ Hamiltonian twice and the stress Hamiltonian once. Consequently, the dependences of the effective masses on stress is not a direct investigation of the evidence of the strain-dependent spin-orbit interaction. The evidence of a spin-dependent deformation potential derives primarily from the difference in deformation potentials measured directly by optical determination of the strain-induced shifts of the Γ_7 and Γ_8 valence bands. Our results are in agreement with a strain-dependent spin-orbit interaction, but we cannot explain the discrepancy between the experimental results and the theoretical estimated values. In order to clarify this point, more detailed calculations would be needed.

Lastly, coming back to the indirect transitions, the stress-induced $X_6 - X_7$ mixing permits a determination of the ratio $E_3^2/(X_6 - X_7)$ [see Eq. (5)]. The energy separation $(X_6 - X_7)$ has not been measured experimentally. However, from different band-structure calculations[20,36] we can infer a value ~0.5 eV which gives $E_3 = 12.8 \pm 1.4$ eV. This is in satisfactory agreement with the corresponding result $2\mathcal{E}_2^* = 16 \pm 6$ eV reported for silicon by Laude *et al.*[8]

V. CONCLUSION

We have accurately determined all the deformation potentials needed to describe the strain dependence of the Γ_6 conduction band, the Γ_8 topmost valence band, the Γ_7 spin-orbit split-off valence band, and the X_6 lowest conduction band in GaP. Our results include the separation of the orbital and spin-dependent deformation potentials for the valence bands and the measurement of the weak stress-induced interconduction band coupling $(X_6 - X_7)$. The spin-dependent deformation potentials have been obtained for the first time. The orbital and hydrostatic deformation potentials are in good agreement with previously published data. We have not been able to resolve the discrepancy quoted in the literature concerning the difference in pressure coefficient for the indirect transitions obtained from (i) pure hydrostatic pressure measurements and (ii) static uniaxial-stress experiments. We believe that new hydrostatic pressure measurements should be undertaken.

*Centre associé au CNRS
[1]G. L. Bir and G. E. Pikus, *Symmetry and Strain-Induced Effects in Semiconductors* (Wiley, New York, 1974).
[2]M. Chandrasekhar and F. H. Pollak, Phys. Rev. B 15, 2127 (1977).
[3]J. L. Merz, A. Baldereschi, and A. M. Sergent, Phys. Rev. B 6, 3082 (1972).
[4]M. I. Wolfe, H. Kressel, T. Halpern, and P. M. Raccah, Appl. Phys. Lett. 24, 279 (1974).
[5]F. H. Pollak, R. S. Baner, R. D. Burnham, and P. M. Raccah, Nuovo Cimento B 39, 437 (1977).
[6]A. Onton and T. N. Morgan, Phys. Rev. B 1, 2592 (1970).
[7]I. Balslev, J. Phys. Soc. Jpn. Suppl. 21, 101 (1966).
[8]L. D. Laude, F. H. Pollak, and M. Cardona, Phys. Rev. B 3, 2623 (1971).
[9]G. Poiblaud, Congrés Annuel de Groupe Francais de Croissance Cristalline Université Louis Pasteur, Strasbourg, Novembre 26–28, 1975 (unpublished); also see G. Poiblaud and G. Jacob, Inst. Phys. Conf. Ser. 24, 134 (1975).
[10]T. Nishino, F. Yamano, and Y. Yamakawa, Jpn. J. Appl. Phys. 14, 1885 (1975).
[11]J. Altier, J. Camassel, and H. Mathieu, in *Proceedings of the International Conference on Measurement and Control, Mecco, Zurich, 1977*, edited by M. H. Hanza (Acta Press, Zurich,

1977), p. 65.
[12]D. Auvergne, P. Merle, and H. Mathieu, Phys. Rev. B 12, 1371 (1975).
[13]K. Suzuki and J. C. Hensel, Phys. Rev. B 9, 4184 (1974).
[14]J. C. Hensel and K. Suzuki, Phys. Rev. B 9, 4219 (1974).
[15]See, for example, F. H. Pollak, Surf. Sci. 37, 863 (1973).
[16]R. Weil and W. O. Groves, J. Appl. Phys. 39, 409 (1968).
[17]H. Brooks, *Advances in Electronics and Electron Physics*, edited by L. Marton (Academic, New York, 1955), Vol. 7, p. 85.
[18]J. C. Hensel, H. Hasegawa, and N. Nakayama, Phys. Rev. 138, A225 (1965).
[19]R. Zallen and W. Paul, Phys. Rev. 134, A1628 (1964).
[20]J. R. Chelikowsky and M. L. Cohen, Phys. Rev. B 14, 556 (1976).
[21]B. Welber, M. Cardona, C. K. Kim, and S. Rodriguez, Phys. Rev. B 12, 5729 (1975).
[22]W. Paul, *Proprietes Physiques des Solides sous Pression* (CNRS, Paris, 1970), p. 199.
[23]B. Welber, C. K. Kim, M. Cardona, and S. Rodriguez, Solid State Commun. 17, 1021 (1975).
[24]F. H. Pollak and R. L. Aggarwal, Phys. Rev. B 4, 432 (1971).
[25]L. D. Laude, M. Cardona, and F.H. Pollak, Phys. Rev. B 1, 1436 (1970).
[26]D. Brust and L. Liu, Solid State Commun. 4, 193 (1966).
[27]F. Cerdeira, J. S. Dewitt, V. Rossler, and M. Cardona, Phys. Status Solidi, 41, 735 (1970).
[28]P. J. Melz and I. B. Ortenburger, Phys. Rev. B 3, 3257 (1971).
[29]G. G. Wepfer, F. C. Collins, and R. Euwema, Phys. Rev. B 4, 1296 (1971).
[30]J. C. Slater and G. F. Koster, Phys. Rev. 94, 1498 (1954).
[31]D. J. Chadi and M. L. Cohen, Phys. Status Solidi B 68, 405 (1975).
[32]D. J. Chadi, Phys. Rev. B 16, 790 (1977).
[33]W. A. Harrison and S. Ciraci, Phys. Rev. B 10, 1516 (1974).
[34]We have checked that a d^{-2} dependence is satisfactorily obeyed by the coupling parameters of Ref. 32.
[35]D. E. Aspnes and M. Cardona, Phys. Rev. B 17, 726 (1978).
[36]F. Bassani (private communication).